Galactic outflows and the kinematics of damped Lyman alpha absorbers

Mon. Not. R. Astron. Soc. **000**, 000–000 (0000) Printed 30 August 2010 (MN LATEX style file v2.2)

Galactic outflows and the kinematics of damped Lyman alpha absorbers

Sungryong Hong[1], Neal Katz[1], Romeel Davé[2], Mark Fardal[1], Dušan Kereš[3], Benjamin D. Oppenheimer[4]

[1] *Astronomy Department, University of Massachusetts, Amherst, MA 01003*
[2] *Astronomy Department, University of Arizona, Tucson, MA 85721*
[3] *Harvard-Smithsonian Center for Astrophysics, Cambridge, MA 02138, USA*
[4] *Leiden Observatory, Leiden University, PO Box 9513, 2300 RA Leiden, the Netherlands*

30 August 2010

ABSTRACT

The kinematics of damped Lyman-α absorbers (DLAs) are difficult to reproduce in hierarchical galaxy formation models, particularly the preponderance of wide systems. We investigate DLA kinematics at $z = 3$ using high-resolution cosmological hydrodynamical simulations that include a heuristic model for galactic outflows. Without outflows, our simulations fail to yield enough wide DLAs, as in previous studies. With outflows, predicted DLA kinematics are in much better agreement with observations. Comparing two outflow models, we find that a model based on momentum-driven wind scalings provides the best match to the observed DLA kinematic statistics of Prochaska & Wolfe. In this model, DLAs typically arise a few kpc away from galaxies that would be identified in emission. Narrow DLAs can arise from any halo and galaxy mass, but wide ones only arise in halos with mass $\gtrsim 10^{11} M_{\odot}$, from either large central or small satellite galaxies. This implies that the success of this outflow model originates from being most efficient at pushing gas out from small satellite galaxies living in larger halos. This increases the cross-section for large halos relative to smaller ones, thereby yielding wider kinematics. Our simulations do not include radiative transfer effects or detailed metal tracking, and outflows are modeled heuristically, but they strongly suggest that galactic outflows are central to understanding DLA kinematics. An interesting consequence is that DLA kinematics may place constraints on the nature and efficiency of gas ejection from high-z galaxies.

Key words: quasar: absorption lines, galaxies: formation, galaxies: kinematics and dynamics

1 INTRODUCTION

Damped Lyman alpha systems (DLAs), i.e. H I absorption line systems having column densities of $N_{\rm HI} > 2 \times 10^{20} {\rm cm}^{-2}$ (Wolfe et al. 1986), contain the dominant reservoir of neutral hydrogen in the Universe (see review by Wolfe, Gawiser, & Prochaska 2005). Since neutral hydrogen is closely connected with star formation (e.g. Kennicutt 1998), DLAs represent the neutral gas repository for fuelling star formation. Influential work by Storrie-Lombardi & Wolfe (2000) suggested that the global neutral gas content measured from DLAs declines with cosmic epoch in concert with the growth in cosmic stellar mass. Other studies with different selection methods suggest that the decline in neutral gas is not as steep (Rao, Turnshek, & Nestor 2006). Nevertheless, one expects some connection between galaxies identified in stellar emission and those identified in gas absorption such as DLAs. Studying this connection has been the focus of a large number of investigations, enabled by the ability to routinely catalogue absorbers and galaxies at $z \gtrsim 2$ where optical Lyα absorption line studies have accurately characterised the DLA population.

Despite these efforts, a deep understanding of the relationship between DLAs and emission-selected galaxies remains elusive. Studies of neutral hydrogen absorption around Lyman break-selected galaxies (LBGs) at $z \sim 2-3$ show a wide range of absorption strengths (Adelberger et al. 2005). DLAs have gas-phase metallicities that are lower than that seen in LBGs, and show a much larger spread (Prochaska et al. 2005). Measures of the C II* cooling rates in DLAs indicate that the star formation rates are dramatically lower than that seen in LBGs (Wolfe et al. 2004). Low-redshift imaging of DLAs show a heterogeneous population of generally sub-L_* galax-

ies, but it is unclear if this is relevant to high-z DLAs. On the other hand, the clustering of LBGs and DLAs at $z \sim 2-3$ suggests that they occupy similar halos (Bouché et al. 2005; Cooke et al. 2006). Hence, even though a wealth of observational data exists for DLAs, it cannot be definitively said whether DLAs are lower-mass LBG analogs, whether they are a phase of galaxy evolution that eventually leads to LBGs, or whether they are an altogether separate galaxy population.

One approach for constructing a unified framework for the nature of DLAs is to employ numerical simulations that account for the hierarchical growth of galaxies including gas physical processes and star formation. Early investigations using simulations by Haehnelt, Steinmetz, & Rauch (1998, hereafter HSR98) suggested that DLAs traced clumps of cold gas that were in the process of assembling into a larger galaxies. This proto-galactic clump (PGC) model favoured the interpretation of DLAs as a precursor phase to LBGs. Gardner et al. (2001) used simulations in cosmological volumes to argue that the bulk of DLAs must arise near dwarf galaxies, suggesting that they are low-mass LBG analogs. Maller et al. (2001) used semi-analytic models to argue that DLAs must come from gas distributions within dark halos that are extended relative to that expected from angular momentum support, and hence another mechanism such as tidal stripping may be important for obtaining the correct cross-section for DLA absorption. Nagamine et al. (2007) found that DLA properties are significantly affected by galactic outflows, and argued that the more successful models showed DLAs as being lower-mass analogs of LBGs. Simulations by Razoumov et al. (2006) incorporated radiative transfer to model the neutral gas distribution more accurately, and found that DLAs can arise from a variety of environments, from the centres of small galaxies to filamentary tidal structure in large halos. Pontzen et al. (2008) used hydrodynamic simulations with star formation and outflows together with radiative transfer, and were able to match the column densities and (for the first time) the metallicity range of DLAs. While these successes are impressive, one set of observations have consistently confounded all such models: The kinematic properties of DLAs.

Prochaska & Wolfe (1997, hereafter PW97) observed the detailed kinematics of DLAs via their low-ionization metal lines. They devised four kinematic diagnostics to quantify their findings, the key one being the velocity extent of DLAs. The observations show a pronounced tail to large velocity extents. Such a tail is not seen in simulations, from the earliest models (Prochaska & Wolfe 2001) to the most sophisticated recent ones (Razoumov et al. 2008; Pontzen et al. 2008). In general, to match the observed kinematics the absorption cross section of low-mass halos must be reduced significantly (Barnes & Haehnelt 2009), which does not arise naturally in fully dynamical models.

Fundamentally, the difficulty with all these models is that they yield few absorbers whose velocity spread significantly exceeds the characteristic velocity of the halo in which the system resides. Since early gas-rich galaxies tend to be small, this makes it difficult to reproduce the observed high-velocity ($\gtrsim 200$ km/s) tail in DLA system widths. This implies that the gravitational dynamics of hierarchical assembly alone cannot explain the distribution of the observed kinematics. Hence, any model that does not add a significant component of non-gravitational velocities to the neutral gas seems doomed to fail the DLA kinematics test. Alternatively, the original model of Wolfe et al. (1986), which proposed that DLAs are large, puffy rotating disks, provides an excellent agreement with the observed kinematics, but forming enough such objects by $z \sim 3$ is challenging in currently-favoured cosmologies. Hence the oft-debated claim by Prochaska & Wolfe (1997, 2001) that cold dark matter (CDM) models cannot straightforwardly reproduce the kinematic structure of DLAs remains viable.

While it could be that the currently-favoured hierarchical galaxy formation scenarios are incorrect, their wide-ranging successes in other areas suggest that the explanation probably lies somewhere within the poorly-understood baryonic physics associated with galaxy formation. For DLAs, it has been suggested (e.g. Pontzen et al. 2008) that galactic outflows may be the missing ingredient needed to increase the kinematic widths and to lower the absorption cross-sections of smaller halos. Recent work indicates that essentially all star-forming galaxies at $z \gtrsim 1$ are generating outflows of hundreds of km/s (e.g. Pettini et al. 2001; Steidel et al. 2004; Shapley et al. 2005; Weiner et al. 2009), with mass outflow rates comparable to or more than their star formation rates (Erb et al. 2006; Steidel et al. 2010). Theoretically, outflows are believed to be responsible for suppressing early star formation (Springel & Hernquist 2003b), without which the cosmic stellar mass density would far exceed observations (Davé et al. 2001; Balogh et al. 2001). But it is unclear how such outflows affect DLAs. Their star formation surface densities are quite low (Wolfe et al. 2004), so they may not generate outflows at all. Even if they do, it is unclear how much mass is being carried in outflows, and whether it would result in enhanced DLA kinematic widths in accord with observations. Simulating the impact of outflows on DLA kinematics is a challenging problem, because it requires both redistributing neutral gas accurately as well as self-consistently modeling the energy deposition by outflows into the surrounding gas.

Recently, several groups have considered the impact of outflows on DLA properties, specifically kinematics. Barnes & Haehnelt (2009) used a semi-analytic model to interpret observations of DLAs and faint extended Lyα emitters, and showed that the incidence rate and kinematics of DLAs are best reproduced if neutral gas is removed from halos with circular velocities $\lesssim 50-70$ km/s, suggesting an important role for outflows. Tescari et al. (2009) followed up the work of Nagamine et al. (2007) to assess, among other things, the impact of various outflow models on DLA kinematics, and found that none of their outflow models were able to reproduce the kinematics completely, although a model based on momentum-driven wind scalings came closest. Zwaan et al. (2008) argued from an observational perspective that DLA kinematics must be influenced by outflows, by comparing the H I kinematic widths of local H I galaxies and those of high-z DLAs, and showing that (assuming that locally-identified DLA galaxies are representative of those at high-z) some other process such as outflows must be enhancing the kinematics of high-z DLAs. Hence there is growing evidence that DLA kinematics are strongly impacted by galactic outflows.

In this paper, we investigate whether galactic outflows can both lower the absorption cross-section of small halos

and broaden the velocity widths enough to bring the theoretical DLA kinematics into accord with the observations. To do so, we employ cosmological hydrodynamic simulations of galaxy formation, with the key addition being several heuristic models of galactic feedback. We consider three variants: No outflows; a model with constant outflow speed and mass loading factor (i.e. the mass outflow rate relative to the star formation rate; Springel & Hernquist 2003b, hereafter SH03); and a model where the outflow speed and mass loading factor scale according to expectations from momentum-driven winds (Murray, Quataert, & Thompson 2005). Such momentum-driven wind scalings implemented within our models have proved remarkably successful at reproducing a wide range of observations, including: the observed IGM metal content from $z \sim 0-6$ (Oppenheimer & Davé 2006, 2008, 2009); observations of early galaxy luminosity functions and evolution (Davé, Finlator, & Oppenheimer 2006; Bouwens et al. 2007); the galaxy mass-metallicity relationship (Finlator & Davé 2008); the observed enrichment in various baryonic phases (Davé & Oppenheimer 2007); the metal and entropy content of low-redshift galaxy groups (Davé, Oppenheimer, & Sivanandam 2008); the H I distribution in the local universe (Popping et al. 2009); and the faint-end slope of the present day stellar mass function (Oppenheimer et al. 2010). Momentum-driven wind scalings of outflow velocity are also observed in nearby starburst outflows (Martin 2005; Rupke et al. 2005), providing an intriguing connection between outflows today and in the past. Hence our momentum-driven wind model provides a concrete (albeit phenomenological) model for how outflows are related to the properties of star-forming galaxies across cosmic time.

Our primary result in this paper is that our momentum-driven wind simulation is able to reproduce the observed kinematics of DLAs. Without winds, our simulated DLA kinematics do not show nearly enough wide-separation systems and have an average velocity width that is too small, in agreement with previous studies. A constant wind model, as implemented by Springel & Hernquist (2003b) and used by Nagamine et al. (2007) to study DLAs, improves over the no-wind case but is still unable to statistically match DLA kinematics. The primary reason for the success of momentum-driven wind scalings is that it ejects large amounts of mass from small galaxies, at relatively low velocities such that the gas is not overly heated. Although our simulations are somewhat simplistic, using a heuristic wind prescription, no radiative transfer, and relatively low spatial resolution ($\sim$ 200 pc physical at $z = 3$), they are the first to statistically match the observed DLA kinematics within a cosmological context. The implication is that DLAs represent the extended neutral gas envelopes of early star-forming galaxies that are driving outflows, and furthermore that such outflows are effective at moving large amounts of neutral gas into the regions surrounding early galaxies.

Our paper is organised as follows: In §2 we describe our simulations and methodology for computing DLA absorption. In §3, we present our results for DLA abundances and present statistical tests on the kinematics of each feedback model compared to the observations. We also present many physical properties that relate DLAs to their host galaxies and dark matter halos. We summarise our results in §4.

2 SIMULATIONS

2.1 Input physics

We simulate 8 h^{-1}Mpc periodic cubic comoving volumes using the cosmological tree-particle mesh-smoothed particle hydrodynamics (SPH) code GADGET-2, with modifications including radiative cooling and star formation (Springel & Hernquist 2003a). Our version used in this work (described in Oppenheimer & Davé 2006) also includes metal-line cooling (Sutherland & Dopita 1993), assumes a (spatially-uniform) cosmic photoionising background taken from Haardt & Madau (2001), and includes a heuristic prescription for galactic outflows driven by star formation that we describe in the next section. We focus on $z = 3$ outputs as that is the typical redshift for the DLAs with well-measured kinematics.

We choose cosmological parameters of $\Omega_m = 0.3$, $\Omega_\Lambda = 0.7$, $h = 0.7$, $\sigma_8 = 0.9$, and $\Omega_b = 0.04$ and generate the initial conditions at $z = 199$ using the Eisenstein & Hu (1999) transfer function. These parameters are consistent with the WMAP-1 results (Spergel et al. 2003) but are somewhat different than the latest WMAP-7 results (Komatsu et al. 2008). However, these differences are not expected to affect our general conclusions, as the uncertainties in modeling the baryonic physics probably dominate over these differences. We use 256^3 particles each for the gas and the dark matter, yielding particle masses of $4.84 \times 10^5 M_\odot$ for the gas and $3.15 \times 10^6 M_\odot$ for the dark matter. The equivalent Plummer gravitational softening length is 0.625 h^{-1} comoving kpc, or 223 proper pc at $z = 3$. These simulations resolve star formation in halos down to virial temperature of $\sim 2 \times 10^4$K, below which ambient photoionisation is expected to provide significant suppression of gas accretion. We note that the numerical resolution in our cosmological volume is better than that in the individual halo simulations of HSR98.

2.2 Outflow models

Galactic outflows appear to be related to star formation, but the exact relationship is unknown. While many recent studies have focused on explicitly driving winds by over-pressurising the ISM via supernova heat input (e.g. Stinson et al. 2006; Ceverino & Klypin 2008), it is clear that such processes are sensitive to scales below any realistically achievable resolution within a cosmological volume. Hence SH03 took the approach of explicitly incorporating outflows with tunable parameters, to avoid a strong dependence on physics below the resolution scale.

In the SH03 implementation, an "outflow model" is described by choosing two parameters: the mass loading factor η, and outflow velocity $v_{\rm wind}$. The mass loading factor is defined as $\eta \equiv \dot{M}_w / \dot{M}_\star$, where $\dot{M}_w$ is the mass loss rate by winds and $\dot{M}_\star$ is the star formation rate.

Each gas particle that is sufficiently dense to allow star formation has some probability to either spawn a star particle, or to be kicked into an outflow. The ratio of those probabilities is given by the mass loading factor η. If a particle is selected to be in an outflow, its velocity is augmented by $v_{\rm wind}$, in a direction given by $\pm \mathbf{v} \times \mathbf{a}$ (resulting in a quasi-bipolar outflow).

When a gas particle becomes a wind particle, its hydrodynamic forces are turned off until the particle escapes

the star-forming region and reaches a density of one-tenth the critical density for star formation. The maximum time for hydrodynamic decoupling is 20 kpc divided by the wind speed, ensuring that the hydrodynamic forces will almost always be turned off for less than 20 kpc. At the simulation resolution we employ, our results are not very sensitive to whether or not we decouple (but see Dalla Vecchia & Schaye 2008, who show that it makes a large difference at very high resolution), but it does allow for better resolution convergence. However, this decoupling does imply that the detailed distribution of metals around galaxies may be inexactly modeled owing to the lack of accounting for hydrodynamical effects. For this reason, we will prefer to use the H I distribution directly when computing DLA kinematics, and simply tie the metals directly to the H I. We note that Tescari et al. (2009), using simulations similar in physics and resolution to ours, explored the difference in kinematics between using the metals directly and using the H I distribution with a fixed assumed metallicity, and found that observed kinematics were better reproduced in the latter case, suggesting that some metal diffusion or smoothing may be required. We follow their more optimistic case here, with the hope that future simulations will allow us to more robustly and self-consistently model the metal distribution near galaxies.

SH03 chose $v_{\rm wind}$ and η to be constants, based on observations available at the time (Martin 1999; Heckman et al. 2000). The wind velocity v_w was derived from the supernova feedback energy,

$$\frac{1}{2}\dot{M}_w v_w^2 = \chi \epsilon_{SN} \dot{M}_\star, \quad (1)$$

where ϵ_{SN} is the energy deposition by Type II supernovae per unit of star forming mass, and χ is the fraction of supernovae energy that drives the wind. SH03 set $\chi = 1$, and used $\epsilon_{SN} \sim 4 \times 10^{48}$ erg/$M_\odot$ for a Salpeter initial mass function, yielding a wind velocity of $v_{\rm wind} = 484$ km/s. They set $\eta = 2$ to roughly reproduce the observed present-day mass density in stars. SH03 showed that this wind model produces a cosmic star formation history that is in broadly agreement with observations, and is resolution converged. We will refer to this as the constant wind ("cw") model, since both η and $v_{\rm wind}$ are independent of galaxy size.

Improved recent observations of local starburst outflows suggest that the wind speed is not constant, but is proportional to a galaxy's circular velocity (Martin 2005; Rupke et al. 2005; Weiner et al. 2009). This is suggestive of momentum-driven winds, as worked out analytically by Murray, Quataert, & Thompson (2005). OD06 implement a momentum-driven wind model in a cosmological simulation. In this scenario, the wind speed scales as the galaxy's velocity dispersion σ, and since the momentum deposition per unit star forming mass is assumed to be constant, the mass loading factor is inversely proportional to σ.

For our momentum-driven wind model, we employ

$$v_w = 3\sigma\sqrt{f_L - 1} \quad (2)$$

$$\eta = \frac{\sigma_0}{\sigma}, \quad (3)$$

where f_L is the galaxy luminosity divided by its Eddington luminosity and σ_0 is a normalisation factor. Because our resolution is still too low to compute the galaxy's velocity dispersion, we take $\sigma = \sqrt{-\frac{1}{2}\Phi}$ from the virial theorem, where Φ is the local potential depth where a wind particle is created. The normalisation factor σ_0 is set to 300 km/s as suggested by Murray, Quataert, & Thompson (2005). Values for f_L are taken from observations: Martin (2005) found $f_L \sim 2$, and Rupke et al. (2005) measured $f_L \approx 1.05 - 2$, for local starbursts. In the momentum-driven wind scenario, lower metallicity star formation should produce stronger outflows owing to greater ultraviolet (UV) flux output; we account for this using the stellar models of Schaerer (2003). Specifically, we set

$$f_L = f_{L\odot} \times 10^{-0.0029\times(\log Z + 9)^{2.5} + 0.417694} \quad (4)$$

where $f_{L,\odot}$ is randomly chosen between $1.05 - 2.0$, and Z is the gas particle's metallicity. We term this momentum-driven wind model ("vzw"). In contrast with the cw model, $v_{\rm wind}$ and η depend on galaxy size.

We note that this momentum-driven wind implementation differs from our more recent works (e.g. Oppenheimer & Davé 2009) that use the galaxy mass to calculate σ. However, as we showed in Oppenheimer & Davé (2008), this choice makes little difference at $z = 3$, and only becomes critical at $z \lesssim 2$ when large potential wells with hot gas develop. Furthermore, our implementation also differs from that in Tescari et al. (2009), who use a calibrated relationship to the halo mass to determine σ.

Finally, for comparison we also evolve a model with no galactic outflows (no winds, "nw"). Note that this model still includes thermal supernova feedback within the context of the subgrid multiphase ISM model of Springel & Hernquist (2003a). It is a poor match to many observations, but provides a baseline to assess the impact of outflows. The suite of three models employed here are a subset of those in OD06.

2.3 Distribution of neutral gas

Here we describe how we calculate the distribution of neutral gas in each simulation. There are two significant complications for this: first, in the multi-phase ISM model of Springel & Hernquist (2003a) that we employ, only some fraction of each particle is actually neutral. Second, since we do not perform detailed radiative transfer, we must account for the effects of self-shielding that can mitigate the strength of the photoionising flux.

The first issue is straightforward to handle, at least to a sufficient approximation. In our multi-phase model, each particle above a critical density for fragmentation is assumed to consist of a cold phase at 1000 K plus a hot phase at 10^6 K. The cold phase dominates the mass fraction, ranging between $84 - 100\%$ (for primordial gas). Since we are only interested in the cold phase, we assume all particles above the fragmentation density to have 90% of their mass in the cold phase at 1000 K, and ignore the hot phase. Note that with metal cooling included, the fragmentation scale can depend on particle metallicity (OD06) and the cold mass fraction can range slightly lower, but to the level of approximation required here this is not important. In detail, the cold phase is probably confined to even smaller sub-particle scale clumps, but as long as the overall cross-section of these clumps is close to unity on galactic scales (as is found observationally when examining the H I content of galaxy disks,

e.g. Zwaan et al. 2005), then the assumption of smoothly-distribution gas within the particle seems reasonably valid.

Accounting for self-shielding requires more significant approximations. The observed HI column density distribution shows an excess of absorbing systems with $N(HI) \geqslant 2 \times 10^{20}$ when the distribution is extrapolated from the low column density region populated by the Lyman α forest (Lanzetta et al. 1991; Storrie-Lombardi & Wolfe 2000). This excess has been explained as a self-shielding effect typically causing a sharp transition layer from mostly ionised regions to mostly neutral regions (Murakami & Ikeuchi 1990; Petitjean 1992; Corbelli, Salpeter, & Bandeira 2001). Hence self-shielding is a critical aspect for setting the ionization level of gas in DLAs.

Owing to our lack of a full radiative line transfer treatment of Lyα photons, we resort to a simpler estimate for self-shielding. HSR98 use a pure density criterion which assumed that all the gas with a number density above 0.01 cm^2 is fully self-shielded, while the rest is subject to the full metagalactic UV flux. In reality, such a threshold depends on the size of the collapsed object and the local strength of UV background, and hence should be different at each local position.

Our approach is to have two criteria to identify a gas particle as "self-shielded": a maximum temperature and a minimum density. We choose a single value for each criterion within each wind model, and use the observed abundance of DLAs to constrain this value. We will demonstrate that the DLA abundances are not sensitive the choice of temperature threshold, and that the DLA kinematics obtained using different (reasonable) thresholds do not differ significantly. For densities, we will employ comoving densities of $\rho_\theta = (40, 80)\rho_{\rm crit}$, where $\rho_{\rm crit}$ is the critical density at $z = 0$, as two thresholds that span a reasonable range. These correspond to $(1000, 2000)\bar{\rho}_b$, or a baryon density of approximately $(0.014, 0.028)$ cm^{-3} (physical).

In Table 1 we summarise our models. The names signify the wind model and ρ_θ. Also shown are the DLA number densities per unit redshift, and the number of randomly chosen lines of sight (LOS) in our DLA sample. These LOS will be used to investigate the kinematics of each model. Models in boldface, cw40 and vzw80, are the ones that broadly match the observed number density of DLAs, as we will discuss further in §3.1, while also having an observationally-consistent cosmic star formation rate at $z \sim 3$. When we need to compare these wind models with the no-wind case, we choose nw80 as a representative, although this model produces too many DLAs and strongly overpredicts the cosmic star formation rate. Note that in order to bring the no-wind model into agreement with the number density of DLAs, we need a very high choice of ρ_θ that is likely to be unphysical (in the sense that this density well exceeds the threshold density for our multi-phase ISM model). This further highlights the impact that outflows have in regulating the amount of neutral gas in DLAs and the cosmos.

Table 1.

Name	ρ_θ[a]	dN/dz[b]	$N_{\rm LOS}$[c]	$N_{20{\rm km/s}}$[d]	$N_{30{\rm km/s}}$[e]
nw40	40	0.534	1995	883	404
nw80	80	0.443	1995	716	310
cw40	40	0.244	1995	1199	672
vzw40	40	0.379	1992	1306	973
vzw80	80	0.265	1988	1453	1175

[a]Self-shielding comoving density in units of the $z = 0$ critical density.

[b]Number of DLAs per unit redshift.

[c]Number of lines of sight.

[d]# of DLAs with $\Delta v > 20$ km/s and satisfying eq. 9.

[e]# of DLAs with $\Delta v > 30$ km/s and satisfying eq. 9.

2.4 DLA absorption profiles

We now identify DLAs and calculate the absorption profiles for low-ionisation species. We first perform self-shielding corrections to the neutral gas content of individual gas particles as described in the previous section. To identify DLAs, we make an 8000×8000 H I map projected through the entire simulation volume. We randomly choose 2000 pixels with $N_{\rm HI} > 10^{20.3}{\rm cm}^{-2}$, and compute H I Ly$\alpha$ spectra along lines of sight (LOS). We then identify the individual absorbing region along the LOS that is a DLA. In less than 1% of the cases, the total $N_{\rm HI}$ of any single absorber along the LOS is below the DLA threshold, even though the total column exceeds it; we discard those LOS. The actual numbers of identified DLAs for each model are listed in Table 1.

To obtain DLA kinematics, we attempt to mimic the observational procedure of identifying low-ionisation, relatively unsaturated metal lines that can trace the gas motions. Although we track metal enrichment in our simulations, we choose not to attempt to make spectra from the metals directly. This is because (1) we don't accurately track the ionisation field, and (2) as explained above, the tracking of metals in outflows near galaxies is hampered by limited numerical resolution and explicit hydrodynamic decoupling. Instead, we tie the metal abundance to the H I abundance with values representative of fully neutral gas.

We choose Si II (1808Å) as our representative low-ionisation metal tracer, which was used in HSR98 and is generally a good tracer for DLA kinematics. We assume a uniform silicon abundance of [Si/H]$= -1$, and take the oscillator strength from Tripp, Lu, & Savage (1996). Since the ionisation potentials of Si I and Si II are 8.15 eV and 16.3 eV, respectively, which brackets H I, we assume that SiII is dominant and exists only in self-shielded regions and in cold ISM gas. This gives an abundance of $n_{\rm SiII}/n_{\rm HI} = 3.24 \times 10^{-6}$. We multiply the H I optical depths along each spectrum by this value, along with the oscillator strength difference, to obtain the Si II optical depths, thereby generating spectra from which we can examine DLA kinematics. Our results are not sensitive to the specific abundance and ionization choice, because we are primarily interested in the redshift-space extent of metal systems rather than the strengths of the systems themselves.

Example randomly-chosen spectra are shown in Figure 1. Each panel contains 5 LOS; the locations (in our 8000×8000 grid) and H I column densities are indicated

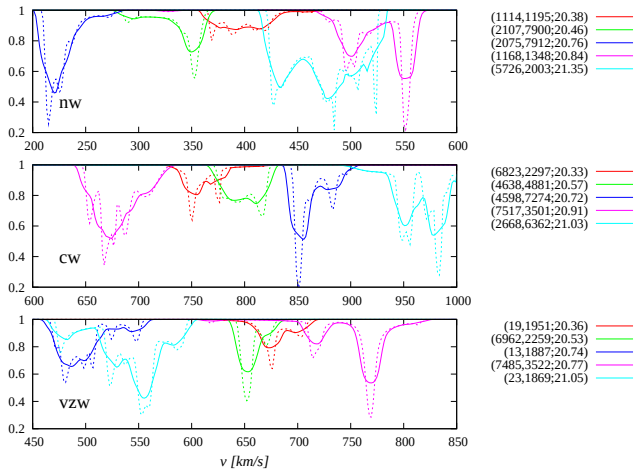

Figure 1. Example low-ionisation metal line (i.e. Si II) spectra drawn from our simulations. The metal optical depths are tied to H I as described in the text. Each colour shows a different LOS; solid and dotted lines show smoothed (19 km/s tophat) and unsmoothed versions, respectively.

along the right side. Such spectra are analyzed as described in §3.2 in order to obtain kinematic statistics for each DLA.

2.5 Identification of galaxies and dark matter halos

Besides DLA kinematics, we are also interested in studying the relationship between DLAs and galaxies in our simulations. Hence, we must identify galaxies in our simulations and we do so using SKID[1] (Katz et al. 1996a), which identifies density watersheds using spline kernel interpolation, and then finds surrounding groups of gas and star particles that are gravitationally self-bound within these density watersheds. We apply SKID to all the star particles and gas particles that satisfy $\rho_{\rm gas}/\bar{\rho}_{\rm gas} > 10^3$ and $T < 30,000$K, and all particles (regardless of temperature) above the multiphase threshold of $\approx 1000\bar{\rho}_{gas}$.

Figure 2 shows the galaxy baryonic mass function for our three simulations We take our galaxy mass resolution limit to be $32m_{\rm SPH} = 1.55 \times 10^7 M_\odot$ (Finlator et al. 2006), shown as the vertical line. This limit appears to be conservative, as the mass function doesn't turn over severely until much lower masses, but detailed resolution testing shows that the individual galaxy star formation histories are poorly converged below this mass owing to stochastic effects and the fact that the densities cannot be adequately resolved. The inflection point in the no-wind case we believe corresponds to the filtering mass (e.g. Gnedin 2000), which is the mass around which galaxies are significantly suppressed by metagalactic photoionization. Galaxies below this mass formed prior to turning on our spatially-uniform ionizing background instantaneously at $z = 9$ (Haardt & Madau 2001). A more realistic radiative transfer simulation would not yield such instantaneous reionization, and would likely not produce such a feature. The wind models have much lower stellar masses for a given halo mass, and hence the

[1] Spline Kernel Interpolative DENMAX; http://www-hpcc.astro.washington.edu/ tools/skid.html

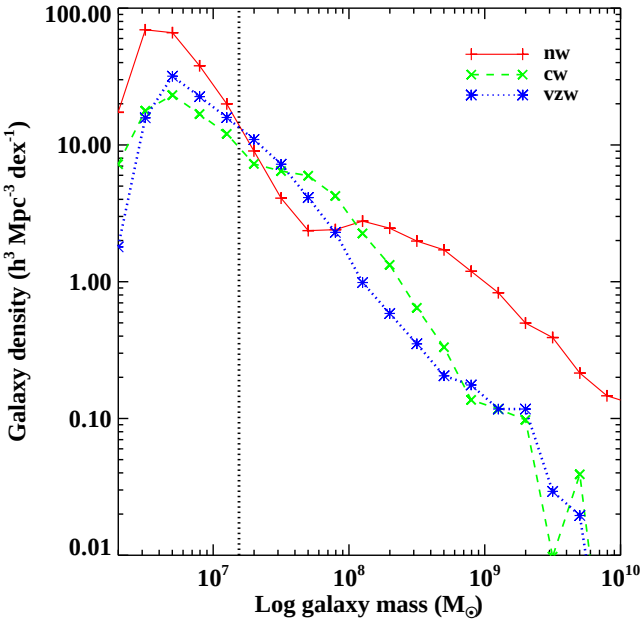

Figure 2. The mass function of gravitationally bound groups found by SKID for the three models: no winds (nw, red solid), constant winds (cw, green dashed) and momentum-driven winds (vzw, blue dotted). We resolve galaxies down to a baryonic mass of $1.55 \times 10^7 M_\odot$, indicated by the vertical dotted line.

effects of filtering are relegated to much smaller masses, at or near our resolution limit. While these effects on the mass function are interesting, they are not immediately relevant to DLAs, so we do not discuss them further.

To identify dark matter halos we use a friends-of-friends(FOF) algorithm (Davis et al. 1985), which finds groups of dark matter particles by linking neighbouring particles within a given linking length. We choose the linking length to be the interparticle distance at one-third of the virial overdensity $\rho_{vir}/\bar{\rho}$, which is the local density at the virial radius for an isothermal sphere, and we take ρ_{vir} from Kitayama & Suto (1996). To define the virial mass, virial radius, and the circular velocity of the dark matter halo we refine the group using a spherical overdensity (SO) criterion. In SO, the halo centre is set to be the location of the most bound FOF particle. Then we expand the radius around this centre until the mean overdensity inside the radius equals $\rho_{\rm vir}/\bar{\rho}$. We define this radius to be $R_{\rm vir}$, the mass within $R_{\rm vir}$ to be $M_{\rm vir}$, and the circular velocity $v_c = \sqrt{GM_{\rm vir}/R_{\rm vir}}$.

In the end, we obtain a sample of about 2000 DLAs and ~ 3000 galaxies within each of our simulations. We will now analyze these systems to understand the impact of outflows on DLA kinematics and the relationship between DLAs and galaxies.

3 PHYSICAL PROPERTIES OF DLAS

3.1 DLA number densities

The observed redshift-space abundance of DLAs, $dN/dz = 0.26 \pm 0.05$ ($z = 3$; Storrie-Lombardi & Wolfe 2000; Prochaska et al. 2005), provides a key constraint for DLA

models. In our case, we use it to constrain our self-shielding criteria, ρ_θ and T_θ. Figure 3 shows our derived abundance for each wind model assuming different ρ_θ and T_θ. Remember that we assume that all gas with a density greater than ρ_θ and a temperature less than T_θ is fully self-shielded. Overall, changing T_θ has little effect on the abundance, while ρ_θ has a large effect.

The no-wind (nw) model has too much neutral gas to match the observations within a large range of choices for ρ_θ. For the two wind models, we choose two self-shielding criteria, $\rho_\theta = 40$ and $\rho_\theta = 80$ for the cw model and the vzw model, respectively, to approximately match the observed dN/dz. A density of $\rho_\theta = 40$ corresponds to $1000\bar{\rho}_b$ and $n_H = 0.014$ cm^{-3} in primordial composition gas, which was adopted in HSR98 as their shielding criteria. So the cw model has the same density threshold value as HSR98 while the vzw model has one twice as large. Our resolution and inclusion of metal line cooling likely affects the choice of threshold values.

Figure 4 shows HI column density maps projected along the x-axis for the nw80, cw40, and vzw80 models. We see substantial differences in the neutral gas distributions produced by these three different feedback implementations. Without winds, the DLA-absorbing gas is highly concentrated within star-forming regions. In the constant wind (cw) case, the absorption is somewhat more extended, but the high outflow velocities generally cause the outflowing gas to be heated, thereby lowering their neutral fractions and hence their densities. The momentum-driven wind model (vzw) produces the greatest extent of high-column density gas. This foreshadows our result that the vzw model will yield the largest DLA kinematic widths.

The more extended gas distribution causes the vzw model to be most sensitive to ρ_θ. This subtle dependence arises because the abundance is sensitive to cross-section, since an extended distribution results in more gas lying near the threshold density. So the curves in Figure 3 partly reflect the different gas topologies that result from the different outflow models. In contrast, the sensitivity to temperature threshold is negligible because most of the gas for any reasonable choice of ρ_θ lies at $\sim 10^4$ K, below which we truncate radiative cooling in our simulations.

As an aside, we note that the filamentary gas structures that are responsible for feeding galaxies with fresh fuel via the cold mode accretion scenario (e.g. Kereš et al. 2005; Dekel et al. 2009) are generally not sufficiently dense to produce DLA absorption, and instead typically have $N_{\rm HI} \lesssim 10^{17}$cm^{-2}. Only in the vicinity of galaxies does the gas starts to self-shield, and the DLAs tend to be confined to even denser gas within and around galaxies.

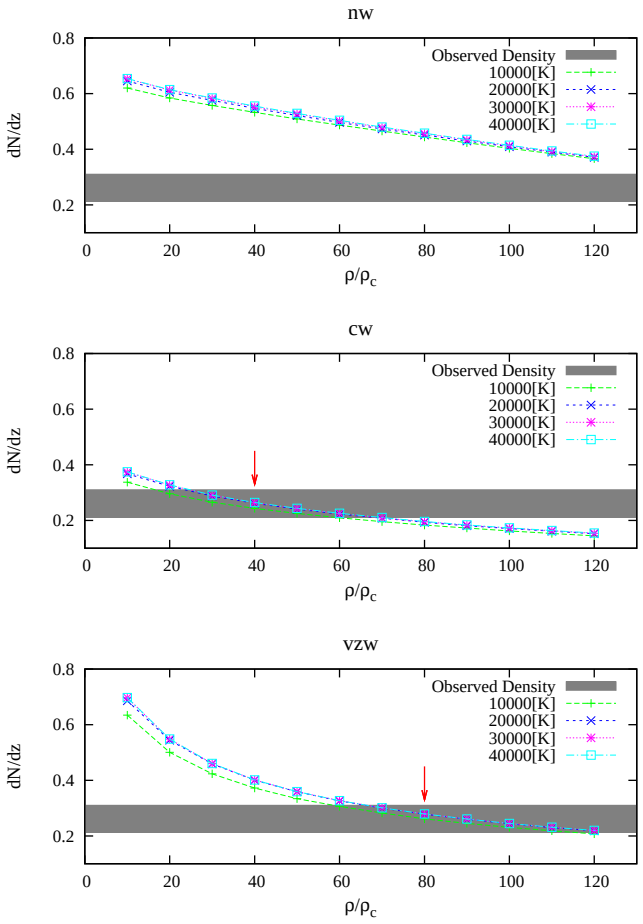

Figure 3. DLA abundances for each model assuming various self-shielding criteria. The temperature dependence is weak, while the density dependence is strong. The red arrows indicate the value we choose for ρ_θ. Note that the values in this figure are slightly larger than the values in Table 1 because we used 2000x2000 maps for this figure and 8000x8000 maps for our main results as presented in Table 1.

3.2 DLA kinematics

We now examine the primary target of our investigation: The kinematics of simulated DLAs and how they compare to observed kinematics. PW97 developed a suite of statistics to descibe the one-dimensional distribution of metal absorption lines within a single DLA. To generate these statistics from our simulated DLAs, we adopt the following procedure:

(i) We select DLAs and then generate Si II absorption lines by tying Si II to H I as described in §2.4.

(ii) We smooth the absorption lines with a 19 km/s tophat window, which is equivalent to the 9-pixel tophat smoothing done in PW97.

(iii) From this profile, we calculate four key quantities, as defined in PW97: The velocities of the largest ($v_{\rm pk}$) and second largest peak absorption ($v_{\rm 2pk}$), the median absorber velocity ($v_{\rm med}$), and the system velocity width (Δv) defined by

$$\Delta v \equiv |v_{95} - v_5|, \quad (5)$$

where v_{95}, v_5, and $v_{\rm med}$ represent the positions at which the optical depths are 95%, 5%, and 50% of the total optical depth. We note that we compute these quantities directly from the Si II optical depths, while PW97 compute them from apparent optical depths obtained from the flux; we expect these quantities to be similar, particularly for the typically unsatured metal lines in DLAs.

(iv) From these quantities, we calculate the DLA kine-

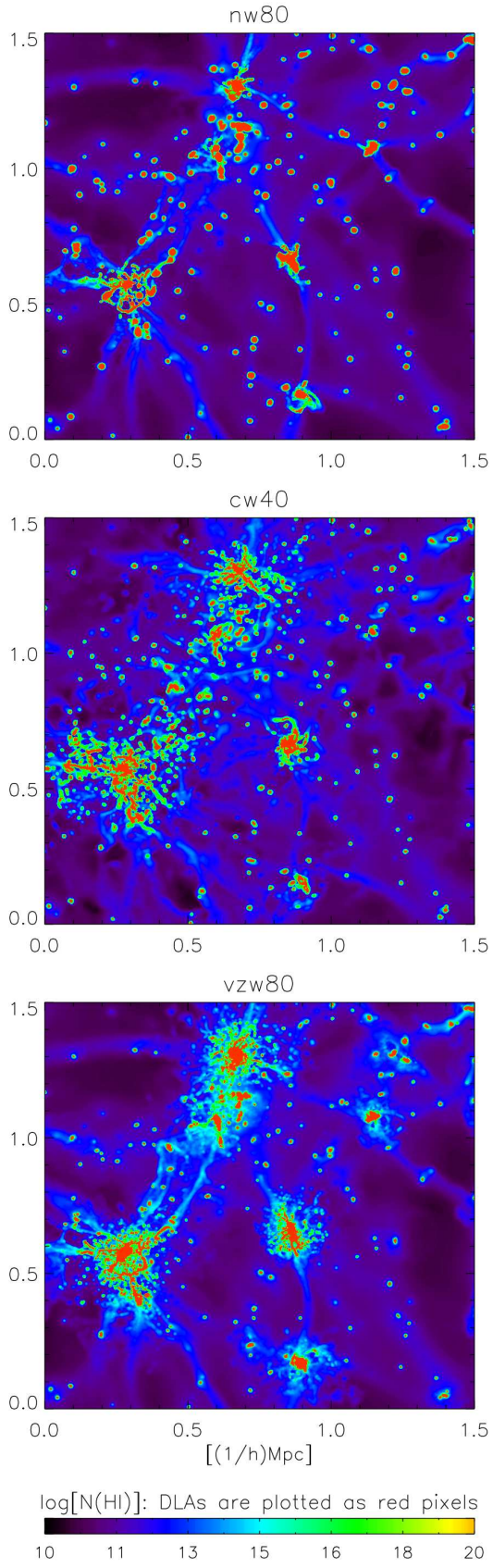

Figure 4. The column density of neutral hydrogen (HI maps) for the no wind model (nw80, top panel), the constant wind model (cw40, middle panel) and the momentum driven wind model (nw80, bottom panel). Every pixel over $2\times10^{20}\mathrm{cm}^{-2}$, i.e. damped absorption, is plotted in red. All lengths are comoving.

matic statistics from PW97:

$$f_{\rm mm} = \frac{|v_{\rm med} - v_{\rm mean}|}{(\Delta v/2)} \quad (6)$$

$$f_{\rm edg} = \frac{|v_{\rm pk} - v_{\rm mean}|}{(\Delta v/2)} \quad (7)$$

$$f_{\rm 2pk} = \pm\frac{|v_{\rm 2pk} - v_{\rm mean}|}{(\Delta v/2)} \quad (8)$$

where the plus sign for the two peak fraction, $f_{\rm 2pk}$, holds if the second peak is between the mean velocity and the first peak velocity; otherwise the minus sign holds. If there is no second peak, we take the edge-leading fraction, $f_{\rm edg}$, for the second peak fraction $f_{\rm 2pk}$. Here, $v_{\rm mean} \equiv \frac{1}{2}(v_{95} + v_5)$.

To avoid saturation effects that blur the kinematic information, and to exclude noise contamination in the observations, we again follow PW97 by only using profiles with peak intensities $I_{\rm pk}$ in the range

$$0.1 \leqslant \frac{I_{\rm pk}}{I_0} \leqslant 0.6 \quad (9)$$

where I_0 is the continuum around the absorption line, or peak optical depths between 0.5 and 2.3. This removes a significant portion of the total DLA sample, roughly 60% for nw, 45% for cw, and 30% for vzw. The variance amongst models in the acceptance fraction based on this criterion suggests that this may be another way to constrain outflow models.

The most crucial statistic is Δv, the system velocity width. It represents the velocity-space extent of the dense neutral absorbing gas, and hence encodes information about internal motions within the ISM as well as any inflow or outflow-induced motions. The other statistics, $f_{\rm mm}$, $f_{\rm edg}$, and $f_{\rm 2pk}$, turn out to be less discriminatory, but we include them for completeness. $f_{\rm mm}$ measures the skewness of the overall absorption in the DLA; a symmetric distribution of optical depths would yield $f_{\rm mm} = 0$. The edge-leading test $f_{\rm edg}$ would be 0 if the strongest absorption is at the kinematic center, but is large if the kinematics are dominated by rotation or infall where the strongest absorption occurs at large velocities from the center. The 2-peak test $f_{\rm 2pk}$ is designed to distinguish between rotation and infall: in the case of rotation, the second peak is expected to be on the same side as the first (and hence yield a positive value), whereas spherical and symmetric accretion would produce the peaks on opposite sides, yielding a negative value (PW97). While these statistics were devised to distinguish between simple scenarios, the complex interplay between infall, outflow, and rotation within a fully hierarchical context precludes such straightforward interpretations. Hence we focus on the distributions of these statistics among DLA samples (both observed and simulated), and use Kolmogorov-Smirnoff (K-S) tests to characterize their (dis)agreement.

In Table 1 we summarise the number of simulated absorption lines, $N_{\rm sample}$, taken from each model. For the observations, we will compare to 46 observed lines of sight from Prochaska & Wolfe (2001). Note that their paper only presented the distribution of Δv; the other quantities were kindly provided by X. Prochaska (private communication).

Before we compare the simulations with the observations, we must consider the issue of velocity resolution effects in the observed DLA sample. The 9 pixel smoothing of

PW97 effectively provides a minimum of $\Delta v_{min} \sim 20$ km/s, and indeed all of the observed DLAs have $\Delta v > 20$ km/s. But HSR98 adopted a minimum threshold of $\Delta v_{min} = 30$ km/s to avoid any possible incompleteness of the DLA sample in the range of $\Delta v = 20 - 30$ km/s. Unfortunately, this threshold can bias the statistics, as it turns out that there are a significant number of smaller halos that host DLAs having Δv within this range. To test this incompleteness issue, we present results for both velocity thresholds of 20 km/s and 30 km/s. However, we note that the observed sample may be significantly incomplete for the 20 km/s threshold, and may not be a fair comparison to the models, hence we prefer to compare to the 30 km/s case. As it happens, our main conclusions are unaffected by this choice.

Figure 5 plots histograms of the four PW97 statistics for our three outflow models, along with their K-S test values as compared to the observed statistics, with $\Delta v_{\rm min} = 30$ km/s. The upper left panel demonstrates the central result of our paper: Models with outflows provide a much better match to PW97's velocity width statistic than our no-wind case. In particular, the momentum-driven wind simulation provides an excellent match to the data with a K-S acceptance level of 0.39, although the constant wind case cannot be definitively ruled out. The rest of the paper will mostly be devoted to understanding the physical origin of the differences among model for the velocity width statistic Δv. We will see that the variations arise because the differences between wind models are most significant for small halos.

The other PW97 tests generally show acceptable K-S values for all models when compared to the data, at least for $\Delta v_{\rm min} = 30$ km/s; at $\Delta v_{\rm min} = 20$ km/s again the vzw case is clearly favored as seen in Table 2. The median-mean statistic $f_{\rm mm}$ (Figure 5, top right) shows that the cw model produces slightly more skewed DLAs than the vzw and nw cases, resulting in marginally poorer agreement in the K-S test, but not so significant as to reject the model. The edge-leading statistic $f_{\rm edge}$ (bottom left) tells a similar story, that nw produces the fewest edge-leading profiles and cw the most, but none of the models can be excluded by the data. The two-peak test (bottom right) shows that most galaxies show rotation signature in their center and interception with infalling or outflowing gas is rare, but it is more frequent for the wind models. This last statistics shows the most disagreement between the simulations and the data, and none of the models are obviously favored. It is unclear why this discrepancy is strongest, since it is a difficult statistic to interpret. However, we note that the thick disk model favoured by PW97 shows a similar distribution, and hence is expected to have roughly the same K-S value.

Our no-wind results are significantly different than HSR98, who found broad agreement with their simulations (without strong outflows) and the data. The discrepancy arises because they extrapolate the relationship between DLA cross-section and halo mass to low halo masses in order to obtain cosmologically-based statistics for their DLA velocity widths. In §3.4.3 we calculate this relationship directly from our simulations, and show that their extrapolation is not valid. Specifically, our no-wind simulation shows considerably increased cross-section over such an extrapolation. This is the main effect that causes our no-wind case to be in poor agreement with data, as compared to HSR98. We note that our numerical resolution is similar to, in fact slightly better than, HSR98. Since HSR98 simulated individual galaxies while we employ a full cosmological simulation, we are able select DLAs based upon their absorption cross-sections to match the observed abundance of DLAs (which HSR98 could not do). This enables us to more accurately characterize the simulated DLA population and more robustly compare it to observations.

Table 2. K-S results

Model	$v_{\rm min}$	$P_{\Delta v}$	$P_{\rm mm}$	$P_{\rm edge}$	$P_{\rm tpk}$
nw40	20	$< 10^{-9}$	$< 10^{-5}$	$< 10^{-6}$	$< 10^{-3}$
nw80	20	$< 10^{-11}$	$< 10^{-7}$	$< 10^{-6}$	$< 10^{-3}$
cw40	20	$< 10^{-6}$	0.0036	$< 10^{-3}$	0.007
vzw40	20	0.18	0.70	0.58	0.14
vzw80	20	0.028	0.14	0.18	0.08
nw40	30	$< 10^{-4}$	0.69	0.19	0.005
nw80	30	$< 10^{-5}$	0.39	0.11	0.03
cw40	30	0.037	0.18	0.81	0.02
vzw40	30	0.51	0.80	0.92	0.04
vzw80	30	0.39	0.91	0.90	0.05

HSR98 also noted that their results depended on the assumed self-shielding criterion. In Table 2 we present the results for different self-shielding criteria as well as for different minimum velocity thresholds. The K-S tests indicate that the vzw model is consistent with the observations for either choice of the threshold density, while the no-wind case is strongly discrepant in Δv regardless of threshold choice. Hence reasonable variations in the self-shielding criteria do not significantly impact our overall conclusions. Hence while it certainly possible to perform more sophisticated self-shielding models even without radiative transfer (e.g. Popping et al. 2009), or even do the full post-processing radiative transfer (Pontzen et al. 2008), we do not expect that this will strongly impact our results.

In summary, galactic outflows appear to be capable of reconciling CDM-based models of galaxy formation with observed DLA kinematics. This is the most important conclusion from our work. Such statistics also provide constraints on wind models, and in the limited tests conducted here we favour momentum-driven wind scalings over constant wind scalings. We now investigate these trends more deeply by studying the properties of galaxies and halos that give rise to DLAs, in order to understand the physical reasons behind the success of outflows in general, and the momentum-driven wind scalings in particular.

3.3 Distance to DLA host galaxies

In our simulations, DLAs are generally associated with galaxies. This is believed to be true in the real Universe, although it is usually only possible to image the host galaxies at low redshifts, where galaxies can be separated from the bright background quasar. On the other hand, DLAs seem to deviate from well-established properties of galaxies such as the Kennicutt-Schmidt relation (Wolfe & Chen 2006). Furthermore, Wolfe et al. (2008) identified a bimodality in DLAs, in which they divide into systems with high and low [CII] 158 μm cooling rates, with the former having proper-

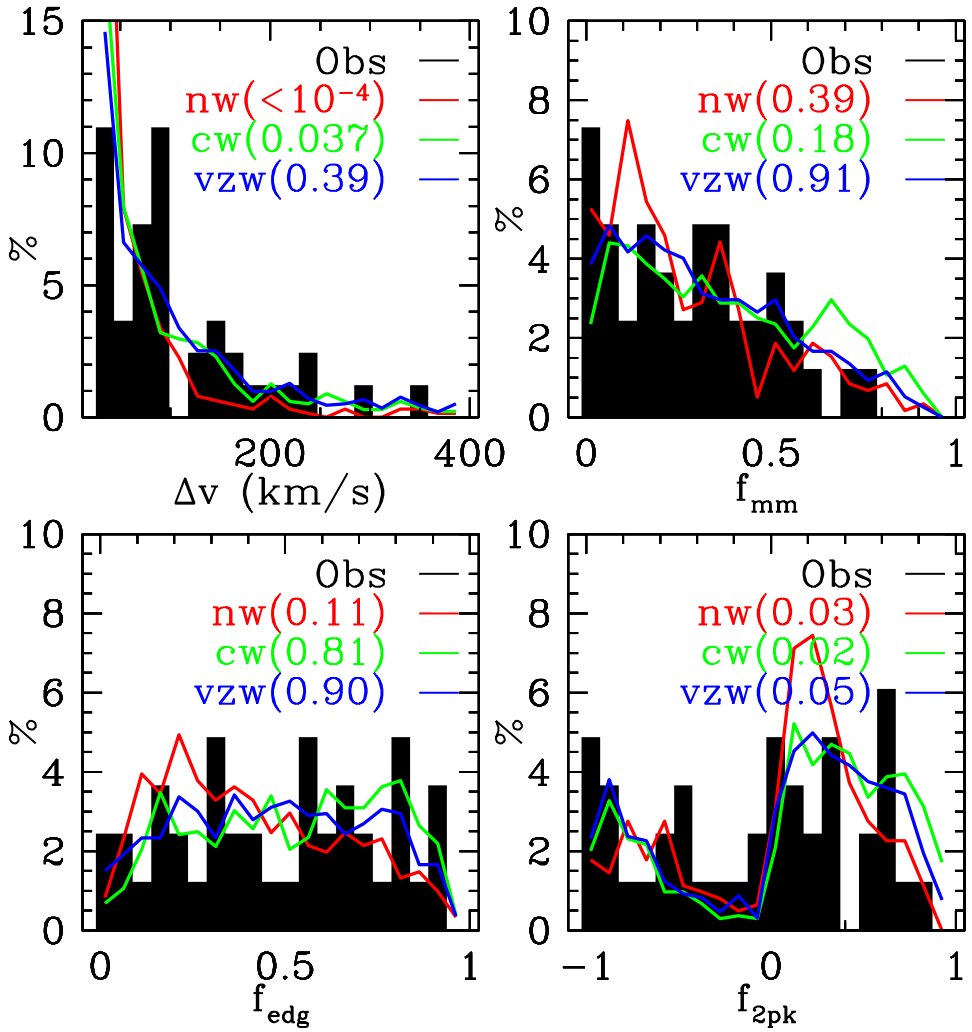

Figure 5. Distributions of the four statistics from PW97 (shaded histogram) compared with the nw80 (red), cw40 (green), and vzw80 (blue) models. A minimum velocity threshold of 30 km/s is assumed. Numbers in parenthesis are K-S test values comparing each model with observations, summarised in Table 2. The no-wind simulations is strongly disfavored, and statistically the vzw model provides better agreement than cw.

ties similar to Lyman Break Galaxies and the latter perhaps arising in a different sort of population. Hence the relation between DLAs and galaxies remains uncertain.

Here we examine some basic properties of the relationship between DLAs and galaxies in our simulations. To connect DLAs to their host galaxies and their host dark matter halos, we need to define the line-of-sight positions of DLAs. Since it is somewhat arbitrary to define the position of diffuse gas, we consider two definitions: $x_{50} \equiv$ the line-of-sight position where 50% of the optical depth is reached; and $x_{\rm ave} \equiv 0.5(x_{30} + x_{70})$, where x_{30} and x_{70} are defined analogously to x_{50}. We also define an uncertainty on the line-of-sight position as $\Delta x \equiv |x_{50} - x_{\rm ave}|$.

In the vast majority of cases, Δx is quite small, so the distance is fairly unambiguous. The few percent of cases where it is not are typically caused by two or more separate gas clumps along the line of sight contributing to a single system. For the remainder of this paper, we will exclude cases where $\Delta x > 0.01$ in units of the simulation box length (i.e. 28.7 proper kpc), since these systems are difficult to relate unambiguously to galaxies. Specifically, this excludes 1.5%, 6.9%, and 3.3% of DLAs in the nw, cw, and vzw cases, respectively. We also examined a tolerance criterion of $\Delta x = 0.001$, with negligible difference in the final results.

The top panel of Figure 6 shows the projected distances, $D_{\rm proj}$, of DLAs versus their column densities for all three models. In general, the median distance is around $\sim$ 2 kpc (distance units are physical unless noted) in all models. There is a weak trend for higher-column systems to arise closer to galaxies. Almost all systems in all cases arise within 10 kpc of a galaxy. Hence in our simulations, DLAs generally arise in the extended neutral gas that are present in and around galaxies at these epochs.

The middle panel shows the cumulative distribution of projected distances, $P(> D_{\rm proj})$, for each wind model. The no-wind case shows a qualitatively different behavior than the wind runs: It shows somewhat larger typical distances at small separations, but beyond $\gtrsim 3$ kpc the nw case shows very few DLAs, while the wind models possess a significant tail to high projected separations. Hence about 95% of the DLAs in the no wind case have distances smaller than 5 kpc, but outflows substantially puff out the neutral gas as shown

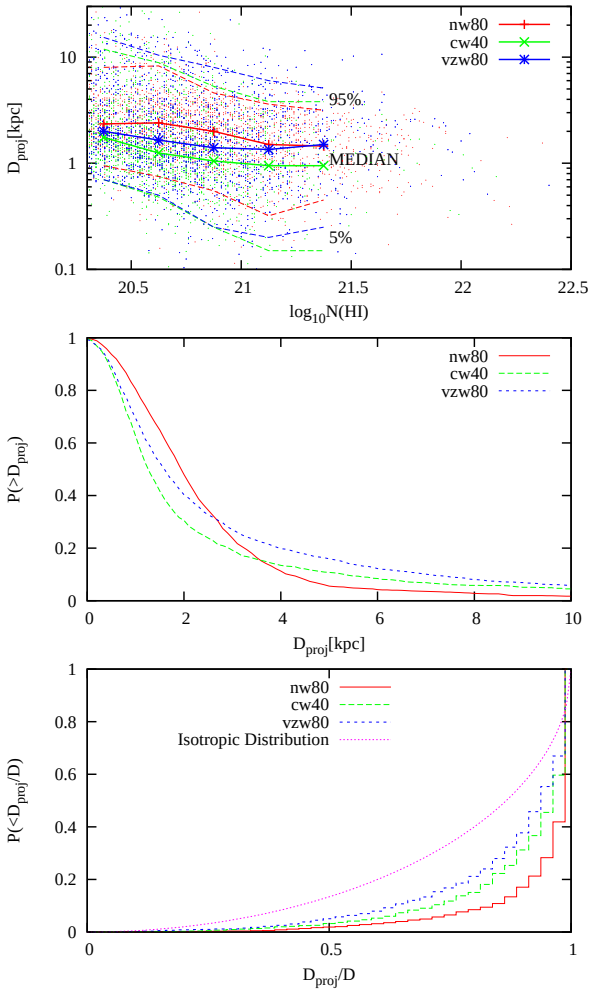

Figure 6. The projected distance, $D_{\rm proj}$, from the host galaxy (top panel), its cumulative distribution (middle panel), and the cumulative distribution of $D_{\rm proj}/D$, which characterises the angular distribution (bottom panel) for the all three models as labelled. The purple dotted curve has the form $1-\sqrt{1-(D_{\rm proj}/D)^2}$, which is what one would expected for an isotropic distribution of small blobs. The no-wind case is closest to having a central blob topology, while winds (particularly vzw) moves the gas distribution closer to isotropic.

in Figure 4, so that in the vzw case 95% of DLAs are within 10 kpc. Since the mass loading factor is larger for small halos in the vzw model than in the cw model, the momentum-driven wind model is most efficient at puffing out the neutral gas from the more numerous and gas-rich small systems.

One can quantify the topology of DLA absorption by examining the ratio of projection distance D_{proj} to real distance D, shown in the bottom panel. First, let us consider some simple illustrative cases: If DLAs come from small blobs that are distributed isotropically from host galaxies, the cumulative distribution should follow the purple dotted line, $P(<D_{\rm proj}/D)=1-\sqrt{1-(D_{\rm proj}/D)^2}$. This is likely similar to a scenario in which DLAs arise from randomly-distributed small disks within a galactic halo, as forwarded by Maller et al. (2001). Conversely, if all DLAs are located in the cross-section plane, then the cumulative distribution should be a step function at a value set by the angle of the plane relative to the line of sight. A special case of this is if the DLA owes to a single, spherical gas blob centered on a galaxy ("central blob"), in which case the distribution will be a step function around unity since $D_{\rm proj}\approx D$.

Now let us examine the actual distributions. The three models generally lie between isotropically-distributed blob and central blob geometries, not surprisingly since these are the extreme cases. In more detail, the no-wind model lies distinctly more towards central blob, because most of the DLA cross-section is concentrated in the central galaxy. Conversely, the wind models follow more closely to the isotropically-distributed blob case, with the vzw case more so than the cw. This means that outflows change the simple centrally-dominated neutral gas topology of the no-wind model to a more complex and extended gas topology. This is consistent with the general impression one gets from examining the H I images in Figure 4.

These topological trends directly correlate with the DLA kinematics examined in §3.2: The more the winds push out gas, the larger the velocity widths. The extra velocity can arise owing to the kinematics of the outflowing gas itself, or else the fact that the gas velocity field typically differs more from the galaxy systemic velocity as one goes farther out into the halo; we dissect these scenarios further in the next section. In either case, the effectiveness by which the momentum-driven winds push out gas into the halo, owing largely to the high mass loading factors in small galaxies, is critical for yielding its agreement with DLA kinematics.

3.4 Relations between DLAs, host galaxies, and host dark matter halos

3.4.1 The environment producing high-Δv DLAs

As pushing out the gas distribution into the surrounding halo seems to be an important aspect of reproducing DLA kinematics, we now investigate how halo environments impact the kinematics of DLAs. Figure 7 shows the relations between the velocity widths of DLAs, Δv and the mass of nearest galaxy $M_{\rm gal}$ (top panel), the distances from the nearest galaxy D (second panel), the circular velocity of the host dark matter halo v_c (third panel), and the mass of the dark matter halo $M_{\rm halo}$ (bottom panels) for the no-wind (red points) and the momentum-driven wind (blue points) models. The constant wind case is not shown for clarity, as its trends are intermediate between the two displayed cases.

The $M_{\rm gal}-\Delta v$ plot shows that Δv does not have a simple relation to the mass of the host galaxy. The nw model shows no significant trend, while the vzw model shows an interesting bimodal distribution for high velocity width DLAs, in which the nearest galaxies tend to be the most massive or the least massive. We will see below that these large-Δv systems tend to occur in massive halos, and hence we can deduce that the high-velocity tail in the vzw model occurs primarily around either massive (likely central) galaxies or low-mass galaxies within a massive halo. Overall, more of the absorption seems to come from low-mass galaxies in the vzw case, showing that the high mass loading factor in small systems produces significantly more DLA-absorbing cross section from these galaxies.

The $D-\Delta v$ plot shows that the highest velocity widths

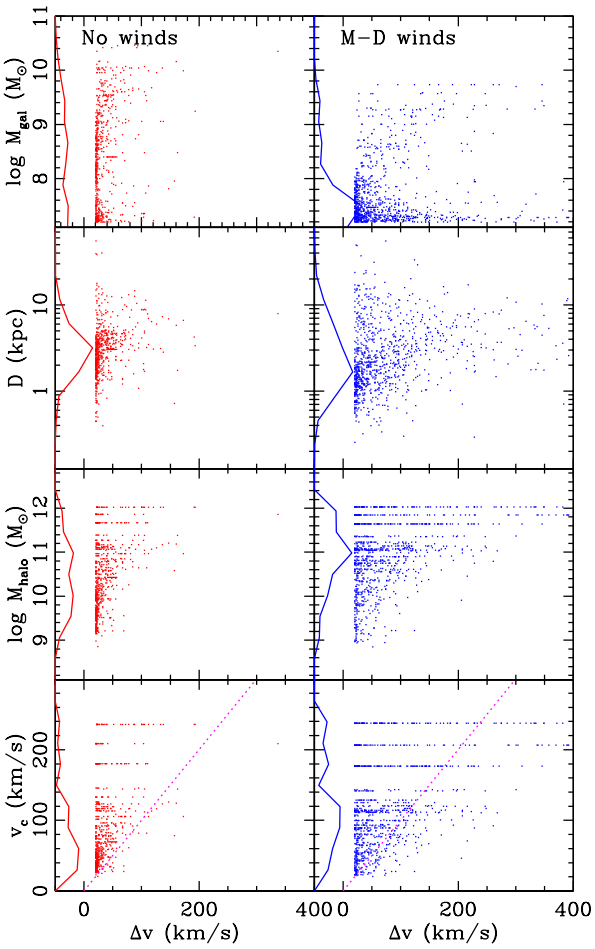

Figure 7. The velocity width of a DLA, Δv, versus the masses of the nearest galaxy (top panel), the distances from the nearest galaxy (second), and the mass (third) and circular velocity (bottom) of the host dark matter halo. Red points show the nw80 model, blue points the vzw80 model. Histograms along the y-axis show the distribution of DLAs along that axis, with a tick mark indicating the median value. In the bottom panel, the dotted line shows $\Delta v = v_c$; DLAs to the right of this have "supergravitational motion", which is more common in vzw compared to nw.

occur relatively far out from the host galaxy, typically $2-10$ kpc away. The overall median distance is approximately 2 kpc for the vzw case and 3 kpc for nw (shown as the tick marks above the vertical histograms), but most of the DLAs with $\Delta v > 150$ km/s lie above these values. This means that if one wants to obtain large Δv values, one has to arrange a significant amount of DLA cross-section at relatively large distances from the host galaxy. At smaller distances, the internal kinematics of galaxies is insufficient to produce large velocity widths. The vzw model, relative to the nw case, clearly produces more DLA-absorbing gas distributed farther away from galaxies.

The $M_{\rm halo} - \Delta v$ plot (third panel) shows an envelope of increasing Δv in larger halos. In the no-wind case, the envelope occurs at roughly an equality between v_c and Δv, showing that with only gravitationally-induced motion, it is rare to produce kinematics larger than the halo circular velocity. Conversely, the vzw case shows significant numbers of DLAs with widths greater than v_c. This is of course key to producing large velocity widths, and we will explore this further in the next section. Note that a massive halo is a necessary but not sufficient condition for large velocity widths, as massive halos can host DLAs with small Δv. These trends are mirrored in the circular velocity panel, which encodes information about the halo radius but otherwise shows very similar trends.

From the above analysis, along with visual impressions from Figure 4, we can assemble a scenario for DLA absorption: Small velocity width DLAs can be produced in all halos, but large velocity widths require a massive halo environment. In the momentum-driven wind scenario, this environment is one where a massive central galaxy is surrounded by numerous small galaxies in a clustered environment. The DLA then occurs at intermediate distances away from the nearest galaxy, which can often be the largest galaxy or one of the smaller systems. The wide DLA velocity widths are then produced either by sightlines intersecting multiple galaxies within a dense region of protogalactic clumps (HSR98; Maller et al. 2001), or by dense gas puffed up by outflows. The former can occur without winds, but the latter requires momentum-driven outflows that produce a puffier neutral gas distribution and raise the H I cross-section of small galaxies within larger halos, thereby yielding the correct fraction of wide systems.

3.4.2 Supergravitational motion

In the no-wind model there is no kinetic energy injection into the neutral gas beyond that provided by gravity. High velocity width DLAs with $\Delta v > v_c$ can still arise owing to merging or infalling motion of neutral gas, as in HSR98, but this is rare. Conversely, outflows provide substantial non-gravitational kinetic energy, which is reflected in the significantly larger fraction of DLAs that have $\Delta v > v_c$ as seen in Figure 7 (fourth panel). We call the kinematics induced by non-gravitational energy "supergravitational motion". The amount of supergravitational motion ($\Delta v > v_c$) therefore quantifies the contribution of wind feedback to the kinematics of the neutral gas.

Figure 8 shows the probability distribution $p(\Delta v/v_c)$ for each model. The probability distribution for the no-wind case is consistent with previous work (Haehnelt et al. 2000). The peak of $\Delta v/v_c$ is around 0.5 and the fraction of systems with supergravitational motion is only 5%. The no-wind case shows a strong maximum at $v/v_c \approx 0.5$, and rapidly drops off to higher v/v_c. The wind models show a qualitatively different behaviour, with a less obvious maximum and a longer tail to high v/v_c. The fraction with supergravitational motion for the cw model and the vzw model are 13% and 22%, respectively. Without such high fractions of supergravitational motion, the models cannot reproduce the incidence of wide DLA velocity widths. Hence the distribution of gas by outflows, together with small-scale galaxy clustering, are critical for explaining DLA kinematics.

3.4.3 DLA cross-section of dark matter halos

To quantify the increase in the puffiness of the gas distribution in the wind models that is responsible for the wider velocity widths, we calculate the DLA cross-sections for each dark matter halo.

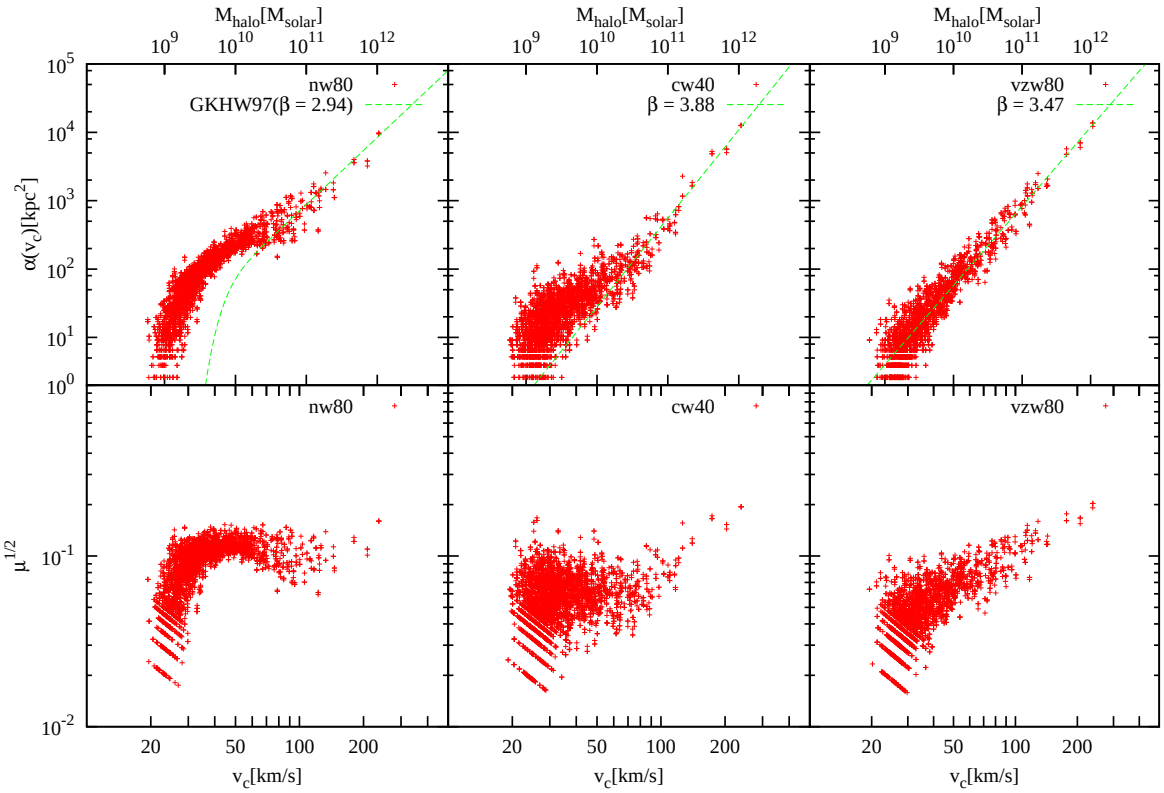

Figure 9. The DLA cross-section α (top panels) and the ratio $\mu \equiv \alpha/\pi R_{vir}^2$ (bottom) as a function of circular velocity v_c for the three wind models. Top axis is labeled by the approximate halo mass. Dashed lines in top panels indicate power-law fits to $v - c > 80$ km/s cross sections. nw80 is consistent with Gardner et al. (1997a) for large halos, and cw40 is consistent with Nagamine et al. (2004); in both cases, there is extra absorption at low v_c relative to an extrapolation from high-v_c. vzw80, in contrast, shows a pure power law with index $\beta = 3.47$ down to the smallest halos. The other two models have a larger cross-section for small halos, which is one reason why they produce too many low-Δv DLAs.

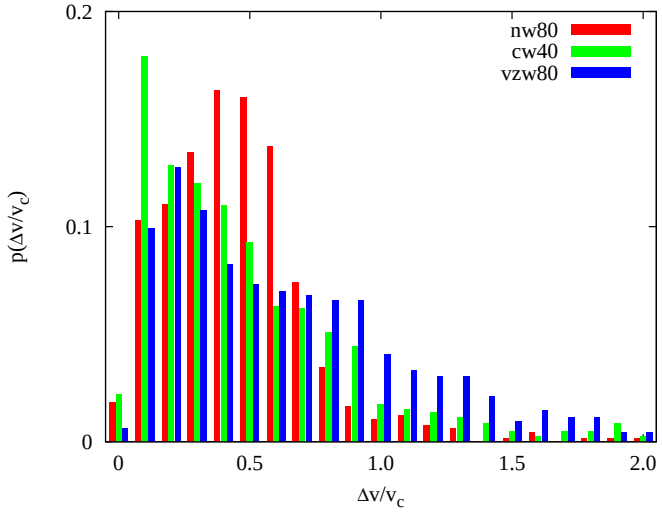

Figure 8. The probability distribution $p(\Delta v/v_c)$ for each wind model. The fraction showing supergravitational motion, i.e.$\Delta v/v_c > 1$, are 5%, 13%, and 22% for the nw model, the cw model, and the vzw model, respectively.

The upper panels of Figure 9 show DLA cross-sections α in comoving kpc^2 for the nw80, cw40, and vzw80 models. We calculate the cross-section from the projected neutral hydrogen maps, including only those pixels that produced DLAs with $\Delta v > 20$ km/s. Each DLA produces 3 points on this plot, for projections along each of the cardinal axes. The relation between α and v_c has traditionally been characterized as a power law with a slope we call β, though as is evident from the plot a pure power-law is only a good description for the vzw80 model (upper right). We note that if the cross-section was proportional to halo mass, then $\beta = 3$, since $M_h \propto v_c^3$ (e.g. Mo, Mao, & White 1998); this turns out to be very roughly the case, though the departures from this are key for understanding DLA kinematics.

The no-wind case shows a relatively shallow power law (i.e. low β) that results in large contributions to DLA cross-section from small v_c systems. This causes a mean velocity width that is too small when the overall DLA abundance is matched. For comparison, we show the fit from the models of Gardner et al. (1997a), which also did not include winds but had much lower spatial resolution. Gardner et al. matched the observed DLA abundance, but in fact the cross-section in small systems was underpredicted compared to our current nw model. Hence, using higher resolution simulations without winds tend to exacerbate the disagreement with observed DLA kinematics.

For the constant wind model, the power law index is $\beta = 3.88$ for $v_c > 80$ km/s. This wind model is identical to that used in Nagamine et al. (2004), but our slope is slightly larger than theirs because we fit the slope for $v_c > 80$ km/s only. We choose this cutoff to highlight where the power

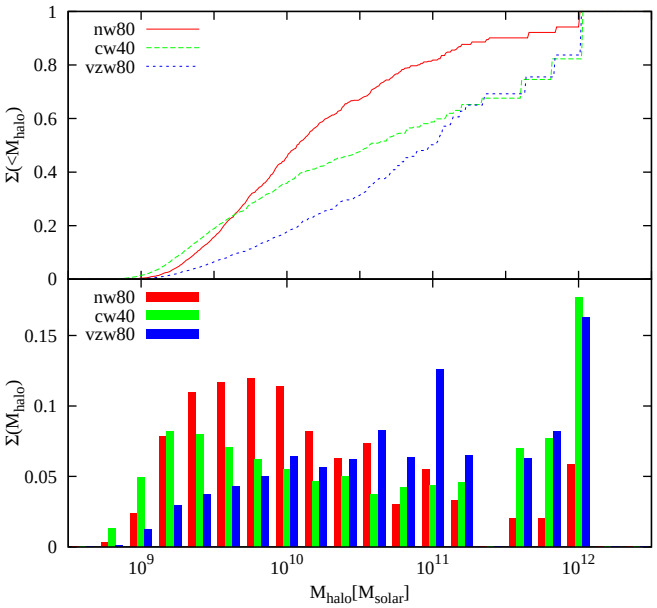

Figure 10. The cumulative global DLA cross-section (top) and the differential global DLA cross-section (bottom).

law breaks in the cw model, especially in relation to the vzw case. For smaller values of v_c, the behaviour of the cw model tends towards that of the no-wind case. Hence the constant-wind case is able to puff out gas to some extent, but still produces significant absorption in low-v_c systems that causes it to match the observed kinematics less well.

Unlike the other two models, the vzw model shows no break in v_c vs. cross section, with an overall slope of $\beta = 3.47$. This low cross-section at small v_c is critical for reproducing the observed kinematics. As argued in PW97 and Prochaska & Wolfe (2001), most CDM galaxy formation models fail to reproduce DLA kinematics because they predict too many small baryonic structures. The key aspect of the vzw model is that it has a high mass loading factor η in small galaxies, which lowers the cross-section of the smaller systems by ejecting more of its material. Indeed, the reduction in cross section is roughly equal to $(1+\eta)$ in smaller halos as expected from simple gas-removal arguments: cw is lower than nw by $\sim \times 3$, and vzw is increasingly suppressed to smaller systems since $\eta \propto v_c^{-1}$.

The lower panels of Figure 9 show $\mu = \alpha/(\pi R_{\rm vir}^2)$, i.e. the ratio of the DLA absorption cross-section to the projected area of the dark halo. For the no wind case μ is almost constant and cuts off rapidly for the smallest halos, and the cw case shows qualitatively similar behavior, lowered by $\sim \times 3$ and with somewhat more scatter. In contrast, in the vzw wind model μ monotonically increases with halo circular velocity, and hence there is relatively more DLA cross-section at larger circular velocities that can give rise to high Δv values.

In Figure 10 we examine the global cross-sections to quantify which halo masses are predominantly responsible for DLA absorption, plotted cumulatively (top) and differentially (bottom) versus halo mass. We define the cumulative global cross section to be

$$\Sigma(< M_{halo}) = \int_0^{M_{halo}} \alpha(M_h) n(M_h) dM_h \qquad (10)$$

The cumulative global cross-section reiterates the result that the vzw model is very efficient at suppressing DLA absorption in small halos relative to larger ones. The cw model produces comparably high cross-sections in large halos to vzw, but it does not suppress the low-mass halo cross-section, and instead its suppression occurs more at intermediate masses.

In summary, the combination of both efficiently suppressing absorption at low masses and having high absorption at large masses relative to the no-wind case is what makes the momentum-driven wind model successful at matching the DLA kinematics. The constant wind case produces the latter requirement but less so the former, making it intermediate between the vzw and no-wind cases.

4 CONCLUSIONS

We examine the kinematic and physical properties of DLAs using cosmological hydrodynamic simulations including three different heuristic prescriptions for how galactic outflow properties are related to their host galaxies: A model without outflows (nw), a constant wind (cw) model where the wind speed of 484 km/s and mass loading factor of 2 are independent of galaxy properties, and a model with momentum-driven wind scalings (vzw) where the wind speed scales as the circular velocity and the mass loading scales inversely with it. Our no-wind model shows results consistent with previous studies of hierarchical models without strong outflows (e.g. Pontzen et al. 2008), and dramatically fails to explain the observed kinematics of DLAs, particularly their systemic velocity widths as traced by low-ionization metal lines. This contrasts with HSR98 who concluded that merging of protogalactic clumps (without winds) can explain the kinematics of DLAs; in our case, the high frequency of wide lines cannot be reproduced when such a model is placed in a cosmological context. Hence without non-gravitational motion, it appears that DLA kinematics are not reproducible within modern hierarchical structure formation models.

We then explored DLA kinematics including outflows. The central result of this paper is that our momentum-driven wind model provides a very good match to all observed DLA kinematic measures, with the possible exception of the 2-peak test that no model matches well. Meanwhile, a model with constant wind speeds and mass loading factors (as in Nagamine et al. 2007) is only marginally consistent with data, and a no-wind case is in strong disagreement with data, particularly in the distribution of DLA velocity widths (Δv) that have historically been difficult to reproduce in CDM-based models. This shows that galactic outflows can reconcile DLA kinematics within current galaxy formation models with observations. Moreover, DLA kinematics could potentially provide interesting constraints on the properties of galactic outflows at high redshifts.

The abundances of DLAs may also provide interesting constraints. Our no-wind case could not reproduce the observed abundances without a very high and likely unphysical threshold density for self-shielding. Meanwhile, both our wind models can match the abundance of DLAs with reasonable choices for this parameter. The previous study of

Gardner et al. (1997a) with no winds matched the observed abundance by an incorrect extrapolation of the DLA cross-section versus circular velocity from low resolution simulations. Our higher-resolution simulations show that such an extrapolation is not valid in the the no-wind or (to a lesser extent) the constant wind case, since these models produce excess cross-section at low-v_c over such an extrapolation. Still, given the crudeness of our self-shielding criterion, it is difficult to assess the robustness of this result. We note that the sophisticated radiative transfer simulations of Pontzen et al. (2008) which include self-consistently driven outflows are able to match DLA number densities (as well as metallicities), but they did not match the kinematics.

To understand why outflows help with DLA kinematics, we investigated the properties of DLA absorption as a function of galaxy and halo properties. A consistent story emerges that momentum-driven winds most efficiently expel gas into a more extended, clumpy distribution around galaxies, particularly for small galaxies living in dense environments. As a result, the DLA cross-section becomes weighted away from small halos (despite arising preferentially in small galaxies) towards more massive halos, where forming structures and outflow-induced motions can yield higher velocities. This results in substantial amounts of super-gravitational motion that directly translates into wide DLA systems.

HSR98 claimed agreement with observed DLA kinematics by noting that their individual DLA simulation produced a velocity width of 60% of the virial velocity $v_{\rm vir}$, and then integrating over the halo mass function assuming that the DLA cross-section scales as $v_{\rm vir}^3$. In our comparable no-wind simulation, this latter scaling is appropriate for larger halos, but it becomes much shallower for smaller ones, yielding much more DLA absorption at small cross sections. This results in poor agreement with the observed kinematics in the no-wind case. In another study, Maller et al. (2001) found that gaseous disks of standard sizes were unable to reproduce DLA kinematics, and that more extended gaseous distributions were required. While they mostly focused on testing extended disks models, they noted that outflows could potentially have a similar effect. Our momentum-driven wind case appears to produce just the required gas distribution. We note that disk sizes are generally too small without strong feedback and much higher numerical resolution than we have here, but the results of Maller et al. (2001) suggest that even optimally conserving angular momentum is not enough, and some supergravitational motion is required. Finally, while outflows produce greater velocity widths, they also produce less cross-section overall. We hypothesize that such models will therefore produce more Lyman Limit Systems (LLS; $10^{17} < N_{\rm HI} < 10^{20.3}{\rm cm}^{-2}$); Davé et al. (2010) showed that winds do produce more strong Lyα forest systems ($N_{\rm HI} > 10^{14}{\rm cm}^{-2}$) at low-$z$, but did not have sufficient statistics to explore LLS. CDM models have traditionally also had difficulty producing enough LLS (e.g. Hernquist et al. 1996), though the strength of the discrepancy has been difficult to quantify owing to uncertainties in measuring column densities in this regime.

More broadly, we note that momentum-driven winds have enjoyed substantial success in reproducing a wide range of observations of early galaxies and intergalactic gas, particularly related to cosmic chemical evolution. On the other hand, this investigation of DLAs focuses solely on the neutral gas; metals are merely used as a tracer of dense H I. Combining these various results leads us to conclude that outflows must move not only metals but also substantial amounts of *mass* around the cosmos. It may be possible to construct a model that enriches the IGM by preferentially expelling highly enriched gas from galaxies which could still reproduce the metal-line kinematics, but the strong low-ionization metal absorption generally indicates a substantial neutral hydrogen component, if for nothing else than to shield it from being sent into higher ionization states. Furthermore, the high mass outflow rates (typically comparable to or greater than the mass forming into stars; Oppenheimer & Davé 2008) suggest that a large amount of ISM gas must be entrained in these outflows, and hence the outflow metallicity cannot be substantially greater than the ambient ISM. Hence it is difficult to envision a scenario where the metals are being ejected highly preferentially compared to the mass. The fact that a single outflow model where vast amounts of gas are expelled at the typical ISM metallicity reproduces all these observations within a cosmological context is quite remarkable. Nevertheless, the lack of possibly important physics in our current simulations precludes any definitive constraints on outflows from DLA kinematics.

DLA kinematics have long been an oddity that did not seem to fit neatly into our current hierarchical view of galaxy formation. Our study suggests that the answer is not in modifications to the hierarchical view, but rather to modifications in the detailed processes of how galaxies form. In a sense, this is a more exciting possibility, as it allows us to move towards constraining such processes from a completely new and different perspective. The work presented here paints a hopeful picture that DLA kinematics may fit into a broader understanding of galactic outflows. However, our current form of modeling outflows is relatively crude, and the present analysis did not address the wider range of DLA observations such as metallicities and redshift evolution that could provide interesting constraints. Furthermore, we did not include detailed radiative transfer to more accurately predict the distribution of neutral gas. Hence this work must be considered as a preliminary step that merely highlights the importance of a new physical process in yielding DLA properties as observed; we plan to examine a more comprehensive suite of DLA properties in the future. This will help us obtain a more complete picture for how DLAs relate to the evolution of galaxies in a hierarchical universe.

REFERENCES

Adelberger, K. L., Shapley, A. E., Steidel, C. C., Pettini, M., Erb, D. K., Reddy, N. A. 2005, ApJ, 629, 636
Balogh, M. L., Pearce, F. R., Bower, R. G., Kay, S. T. 2001, MNRAS, 326, 1228
Barnes, L. A. Haehnelt, M. G. 2009, MNRAS, 397, 511
Bouché, N., Gardner, J. P., Katz, N., Weinberg, D. H., Davé, R., Lowenthal, J. D. 2005, ApJ, 628, 89
Bouwens, R. J., Illingworth, G. D., Franx, M., Ford, H. 2007, ApJ, 670, 928
Ceverino, D. Klypin, A. 2008, arXiv:0712.3285

Cooke, J., Wolfe, A. M., Gawiser, E., Prochaska, J. X. 2006, ApJ, 652, 994
Corbelli, E., Salpeter, E. E., Bandiera, R. 2001, ApJ, 550, 26
Davis M., Efstathiou G., Frenk C. S., White S. D. M., 1985, ApJ, 292, 371
Davé, R., Cen, R., Ostriker, J. P., Bryan, G. L., Hernquist, L., Katz, N., Weinberg, D. H., Norman, M. L., O'Shea, B. 2001, ApJ, 552, 473
Davé, R., Finlator, K., Oppenheimer, B. D. 2006, MNRAS, 370, 273
Davé, R., Oppenheimer, B. D. 2007, MNRAS, 374, 427
Davé, R., Oppenheimer, B. D., Sivanandam, S. 2008, MNRAS, submitted
Davé, R., Oppenheimer, B. D., Katz, N., Kollmeier, J. A., Weinberg, D. H. 2010, MNRAS, accepted, arXiv:1005.2421
Dalla Vecchia, C., Schaye, J. 2008, MNRAS, 387, 1431
Dekel, A. et al. 2009, Nature, 457, 451
Eisenstein, D. J., Hu, W. 1999, ApJ, 511, 5
Erb, D. K., Shapley, A. E., Pettini, M., Steidel, C. C., Reddy, N. A., Adelberger, K. L. 2006, ApJ, 644, 813
Finlator, K., Davé, R., Papovich, C.,Hernquist, L. 2006, ApJ, 639, 672
Finlator, K. & Davé, R. 2008, MNRAS, 385, 2181
Gardner, J. P., Katz, N., Hernquist, L., Weinberg, D. H. 1997, Apj, 484, 31
Gardner, J.P., Katz,N., Hernquist, L., Weinberg,D.H. 2001, ApJ, 559, 131
Gnedin, N. Y. 2000, ApJ, 542, 535
Haardt, F., Madau, P. 2001, in proc. XXXVIth Rencontres de Moriond, eds. D.M. Neumann, J.T.T. Van.
Haehnelt, M.G., Steinmetz, M., Rauch, M. 1998, ApJ, 495, 647 (HSR98)
Haehnelt, M.G., Steinmetz, M., Rauch, M. 2000, ApJ, 534, 549
Heckman, T. M., Lehnert, M. D., Strickland, D. K., Armus, L. 2000, ApJS, 129, 493
Hernquist, L., Katz, N., Weinberg, D.H., Miralda-Escudé, J. 1996, ApJL, 457, L51
Katz, N., Weinberg, D. H., Hernquist, L. 1996, ApJS, 105, 19
Katz, N., Weinberg, D. H., Hernquist, L., Miralda-Escudé, J. 1996, ApJ, 457, L57
Kaufmann, G., Charlot, S. 1994, ApJ, 430, L97
Kennicutt, R. C. 1998, ApJ, 498, 541
Kereš, D., Katz, N., Weinberg, D. H., Davé, R. 2005, MNRAS, 363, 2
Kitayama, T., Suto, Y. 1996, ApJ, 469, 480
Komatsu, E. et al. 2008, ApJS, submitted, arXiv:0803.0547
Lanzetta, K. M., Wolfe, A. M., Turnshek, D. A., Lu, L., McMahon, R. G., Hazard, C. 1991, ApJS, 77, 1
Martin, C. L. 1999, ApJ, 513, 156
Martin, C. L. 2005, ApJ, 621, 227
Maller, A. H., Prochaska, J. X., Somerville, R. S., Primack, J. R. 2001, MNRAS, 326, 1475
Mo, H. J., Mao, S., White, S. D. M. 1998, MNRAS, 295, 319
Murakami, I., Ikeuchi, S. 1990, PASJ, 42, L11
Murray, N., Quataert, E., Thompson, T. A. 2005, ApJ, 618, 569
Nagamine, K., Springel, V., Hernquiest, L. 2004, MNRAS, 348, 421
Nagamine, K., Wolfe, A. M., Hernquist, L., Springel, V. 2007, ApJ, 660, 945
Oppenheimer, B.D, Davé, R.2006, MNRAS, 373, 1265
Oppenheimer, B.D, Davé, R.2008, MNRAS, 387, 587
Oppenheimer, B.D, Davé, R.2009, MNRAS, 395, 1875
Oppenheimer, B. D., Davé, R., Kereš, D., Katz, N., Kollmeier, J. A., Weinberg, D. H. 2010, MNRAS, 860, in press
Petitjean, P., Bergeron, J., Puget, J. L. 1992, A&A, 265, 375
Pettini, M., Shapley, A. E., Steidel, C. C., Cuby, J.-G., Dickinson, M., Moorwood, A. F. M., Adelberger, K. L., Giavalisco, M. 2001, ApJ, 554, 981
Pontzen, A. et al. 2008, MNRAS, 390, 1394
Popping, A., Davé, R., Braun, R., Oppenheimer, B. D. 2009, A&A, 504, 15
Prochaska, J.X., Wolfe, A.M. 1997, ApJ, 487, 73 (PW97)
Prochaska, J.X., Wolfe, A.M. 2001, ApJ, 560, L33
Prochaska, J.X., Herbert-Fort, S., Wolfe, A. M. 2005, ApJ, 635, 123
Rao, S. M., Turnshek, D. A., Nestor, D. B. 2006, ApJ, 636, 610
Razoumov, A. O., Norman, M. L., Prochaska, J. X., Wolfe, A. M. 2006, ApJ, 645, 55
Razoumov, A. O., Norman, M. L., Prochaska, J. X., Sommer-Larsen, J., Wolfe, A. M., Yang, Y.-J. 2008, ApJ, accepted, arXiv:0710.4137
Rupke, D. S., Veillaux, S., Sanders, D. B. 2005, ApJs, 160, 87
Schaerer, D. 2003, A&A, 397, 527
Shapley, A. E., Steidel, C. C., Erb, D. K., Reddy, N. A., Adelberger, K. L., Pettini, M., Barmby, P., Huang, J. 2005, ApJ, 626, 698
D. N. Spergel *et al.*, ApJS, 148, 175
Spergel, D. N., et al. 2006, astro-ph/0603449
Springel, V., Hernquist, L. 2003, MNRAS, 339, 289
Springel, V., Hernquist, L. 2003, MNRAS, 339, 312 (SH03)
Springel, V. 2005, MNRAS, 364, 1105
Steidel, C. C., Shapley, A. E., Pettini, M., Adelberger, K. L., Erb, D. K., Reddy, N. A., Hunt, M. P. 2004, ApJ, 604, 534
Steidel, C. C., Erb, D. K., Shapley, A. E., Pettini, M., Reddy, Bogosavljevic, M., Rudie, G. C., Rakic, O. 2010, ApJ, 717, 289
Steinmetz, M. 1996, MNRAS, 278, 1005
Stinson, G., Seth, A., Katz, N., Wadsley, J., Governato, F., Quinn, T. 2006, MNRAS, 373, 1074
Storrie-Lombardi,L.J., Wolfe, A. M. 2000, ApJ, 543, 552
Sutherland, R. S., Dopita, M. A. 1993, ApJS, 88, 253
Tescari, E., Viel, M., Tornatore, L., Borgani, S. 2009, MNRAS, 397, 411
Tripp, T. M., Lu, L., Savage, B. D. 1996, ApJS, 102, 239
Weiner, B. J. et al. 2009, ApJ, 692, 187
Wolfe,A.M., Turnshek,D.A., Smith, H.E., Cohen, R.D. 1986, ApJS, 61, 249
Wolfe,A.M., Lanzetta, K.M., Foltz,C.B., Chaffee, F.H. 1995, ApJ, 454, 698
Wolfe, A. M., Howk, J. C., Gawiser, E., Prochaska, J. X., Lopez, S. 2004, ApJ, 615, 625
Wolfe,A.M., Gawiser,E., Prochaska,J.X. 2005, ARA&A, 43, 861

Wolfe, A.M., Chen, H.S. 2006, ApJ, 652, 981
Wolfe, A. M., Prochaska, J. X., Jorgensen, R. A., Rafelski, M. 2008, ApJ, 681, 881
Zwaan, M., van der Hulst, J. M., Briggs, F. H., Verheijen, M. A. W., Ryan-Weber, E. V. 2005, MNRAS, 364, 1467
Zwaan, M., Walter, F., Ryan-Weber, E., Brinks, E., de Blok, W. J. G., Kennicutt, R. C. 2008, AJ, 136, 2886